Interfacial effects of Al termination on spin transport in magnetic tunnel junctions

T. Tzen Ong,[1,2] A. M. Black-Schaffer,[1,*] W. Shen,[3,2] and B. A. Jones[2]
[1]*Department of Applied Physics, Stanford University, Stanford, California 94305, USA*
[2]*IBM Research Division, Almaden Research Center, San Jose, California 95120, USA*
[3]*Department of Physics, Georgetown University, Washington, DC 20057, USA*
(Received 22 October 2009; revised manuscript received 22 June 2010; published 27 August 2010)

Experiments have shown that the tunneling current in a Co/Al_2O_3 magnetic tunneling junction (MTJ) is positively spin polarized, opposite to what is intuitively expected from standard tunneling theory which gives the spin polarization as exclusively dependent on the density of states (DOS) at E_F of the Co layers. Here we report theoretical results that give a positive tunneling spin polarization and tunneling magnetoresistance (TMR) that is in good agreement with experiments. From density-functional theory (DFT) calculations, an Al-rich interface MTJ with atomic-level disorder is shown to have a positively polarized DOS near the interface. We also provide an atomic model calculation which gives insights into the source of the positive polarization. A layer- and spin-dependent effective-mass model, using values extracted from the DFT results, is then used to calculate the tunneling current, which shows positive spin polarization. Finally, we calculate the TMR from the tunneling spin polarization which shows good agreement with experiments.

DOI: 10.1103/PhysRevB.82.054429 PACS number(s): 72.25.Mk, 73.40.Gk, 73.40.Rw, 72.10.Bg

I. INTRODUCTION

The discovery of large tunneling magnetoresistance (TMR) in magnetic tunneling junctions[1] (MTJs) has prompted great interest in developing these devices for applications such as magnetic random access memories and magnetic sensors (for reviews, see, e.g., Refs. 2 and 3). The TMR should, in an ideal system, be closely related to the spin polarization of the two ferromagnetic layers sandwiching the insulator, and is typically given by the Julliere model[4] as

$$\mathrm{TMR} \equiv \frac{R_{AP} - R_P}{R_{AP}} = \frac{2P_1P_2}{1 + P_1P_2}. \quad (1)$$

Here R_{AP} and R_P denote the resistance for the antiparallel and parallel alignments of the ferromagnetic layers, respectively, and P_i ($i=1$ and 2) are the bulk magnetic moments of the two layers. This model is based on the assumption that the spin polarization of the tunneling current, which determines the TMR, is an intrinsic property of the spin polarization in the ferromagnetic layers. Experimental results, however, do not often match this phenomenology. Most importantly, for the ferromagnetic $3d$ metals such as Co, which have a negative spin polarization at the Fermi level, the measured spin polarization across an alumina, Al_2O_3, insulating barrier is positive.[5] Experiments have also demonstrated a strong dependence of spin transport on the detailed structural and electronic nature of the insulating layer and its interface with the ferromagnetic layers.[6,7]

Density-functional theory (DFT) calculations of O-terminated interfaces have shown a positive spin polarization for barrier distances beyond 10 Å.[8,9] Additional DFT work have shown that additional oxygen atoms absorbed at the interface form strong Co-O bonds and give rise to a positive spin interface band. This band was found to be dominant in the tunneling process and gives rise to a positive spin polarization of the tunneling current.[10] Formation of an O-terminated interface with Co-O bonds is obtainable by moderate to long oxidation times of the Al_2O_3 layer. An increased magnetization of the interface Co atoms was found to coincide with the optimum TMR using x-ray magnetic circular dichroism measurements.[11] However, one recent experiment failed to detect any induced magnetic moment on the interface O atoms,[12] which should also be present. Hence, details of the physical nature of O-terminated MTJs remains open.

In this work we will instead focus on clean Al-terminated and disordered Al-rich interfaces which are experimentally accessible by not overoxidizing the junction.[13] Earlier DFT results on Al-terminated junctions have shown that the magnetic moment on the Co interface atoms is somewhat reduced by charge transfer and screening effects[8] but Al-rich junctions have not yet been studied nor have the positive spin polarization been explained in any of these junctions. We show here that increasing Al content at the interface can cause dramatic changes in the spin polarization of both the interface region and the tunneling current, even to the degree of changing the sign of the spin-polarized tunneling current as measured experimentally. This explicitly demonstrates that oxygen absorption is not the only means to achieve positive spin polarization as was recently suggested.[10]

More specifically, we use DFT to model $Co/Al_2O_3/Co$ magnetic tunnel junctions with varying Al-rich interfaces to determine atomic structure, band structure, and local-density of states (LDOS). The DFT results explicitly show the importance of the proximity effect on the LDOS of the interfacial layers. The LDOS near E_F of the interfacial Co layer leaks into the first Al layer of the insulating barrier, and gives rise to a small but finite DOS near E_F, hence metallizing the Al layer, as has been seen experimentally.[13] The Al layer also picks up a small ferromagnetic moment due to this proximity effect. Similarly, the LDOS and the spin polarization of the nearest Co layer is reduced. Thus, the spin DOS changes as we cross the interface and the spin polarization actually becomes positive for Al-rich interfaces.

The difference between spin polarization of the LDOS versus that measured in transport was pointed out in an im-

portant work by Mazin.[14] We see similar physics in this system, where the spin polarization of the LDOS at E_F, $\rho(E_F)$, is negative in the bulklike Co(1) layers, whereas the tunneling current is positively spin polarized. We are also able to show that there is a change in the spin polarization of $\rho(E_F)$ from negative in the bulklike layers, to positive in the interfacial layers, which directly leads to a smaller transmission coefficient for the spin-down electrons. This gives physical insight into the relationship between the spin polarization of $\rho(E_F)$ and the tunneling current.

We use a position-dependent effective-mass model to explicitly calculate the spin polarized tunneling current of our junctions. The change in the effective mass of the different bands between the electrode bulklike layers and the interfacial layers result in better matching between the spin-up bands, compared to the spin-down bands. There is then less reflection at the interface, and hence a larger transmission coefficient for the spin-up bands ultimately resulting in a positive spin-polarized tunneling current in the Al-rich junctions.

The paper is organized as follows. In Sec. II we review the details specific to the DFT calculations. We also present the different interface structures we have studied. In Sec. III we report the results for the clean Al-terminated interface as a baseline for the Al-rich interfaces. In Sec. IV we discuss interfacial scattering by excess Al atoms before we present DFT results for disordered, Al-rich interfaces in Sec. V. Finally in Sec. VI we explicitly calculate the spin-polarized tunneling current and the TMR based on the DFT LDOS and band-structure data.

II. DFT COMPUTATIONAL DETAILS

To model the $Co/Al_2O_3/Co$ magnetic tunnel junction we have created $Co/Al_2O_3/Co$ supercells with various Al-terminated interfaces. Thin-film Co is predominantly found in the fcc phase and experimentally it has been found that alumina grows on top of the (111) plane of fcc Co.[7] We have chosen a 2×2 surface unit cell of (111) fcc Co with the theoretical lattice parameter $a=3.38$ Å($a_{exp}=3.55$ Å) as the base structure. In order to enforce bulk conditions in the inner cobalt layers we fix the atomic positions for the three innermost Co layers. As can be seen in Figs. 1 and 5 the relaxed Co layers still closely resemble the constraint layers and thus this relaxation procedure should yield accurate results despite the finite unit cell. For the tunneling barrier we use one unit cell of α-Al_2O_3 (corundum) with the [0001] orientation and Al termination to model the experimentally amorphous alumina. This structure contains four Al layers with three O layers in between them. Since alumina is grown on top of cobalt we adjust the lateral dimensions of alumina to that of the cobalt. This is the same crystallographic orientation as used in previous DFT studies[8–10] and gives an experimental lattice mismatch of only 6% between the cobalt and alumina. While most previous theoretical work have focused on oxygen-rich interfaces there also exist experimental data showing Al termination at the Co/Al_2O_3 interface.[13] We investigate both the clean, abrupt interface with Al termination, see Fig. 1, and two different cases of Al-rich interfaces.

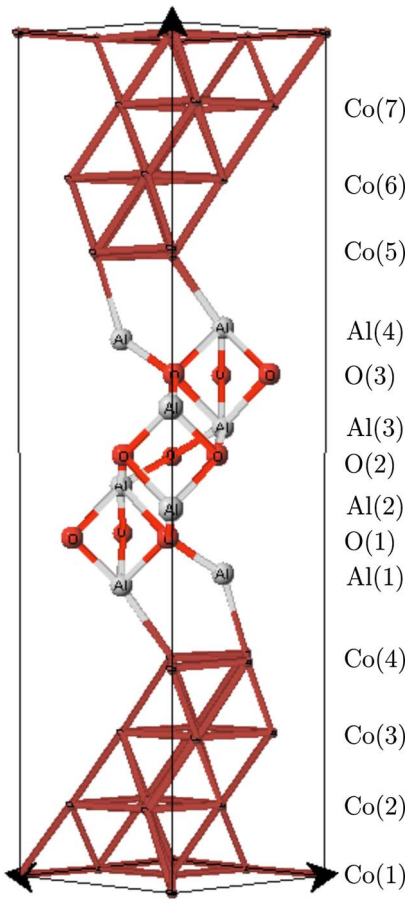

FIG. 1. (Color online) Atomic structure of the clean Al-terminated interface junction. The unit vectors for the supercell as well as the layer identification tags are shown. Layers Co(1), Co(2), and Co(7) were kept fixed in order to impose bulk Co conditions.

The first case has one mixed interface layer with a 1:1 Al to Co ratio. The second case has two mixed layers with a 3:1 and 1:1 Co to Al ratio, respectively, see Fig. 5. We will present the results for the clean interface system in Sec. III and the results for the disordered interface system with two mixed layers in Sec. V. We found the results for the system with one mixed layer to be an interpolation of the clean and two mixed layer interfaces.

The band structure and LDOS were calculated using the first-principles DFT pseudopotential method implemented in the Vienna *ab initio* simulation package (VASP).[15] We have used ultrasoft pseudopotentials and employed both the local-density approximation (LDA) and the generalized gradient approximation (GGA). In general, we expect the LDA calculations to underestimate the lattice constant and the band gap whereas GGA calculations sometimes overcompensate for the LDA error. Thus GGA calculations often results in less consistent errors which is somewhat problematic when studying trends, as we have also found in this work. The cut-off energy for the plane-wave expansion was set to 29 Ry. After k-point convergence tests we chose a $9\times9\times1$ Γ-centered k-point sampling. The atomic structure, except the fixed three innermost Co layers, was relaxed until the change in total energy between two ionic steps was less than

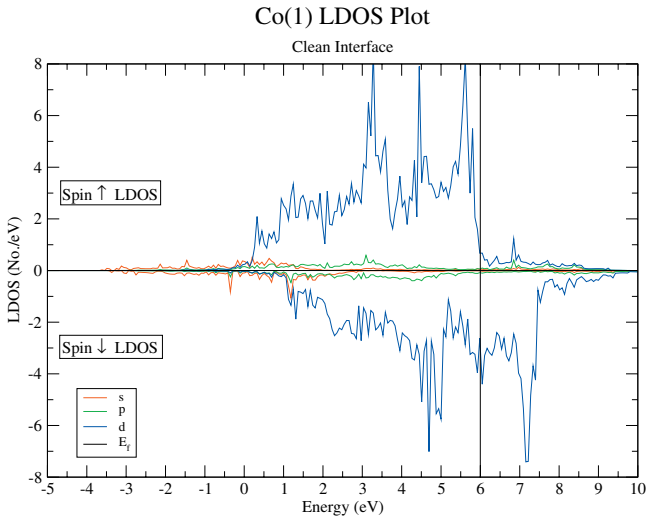

FIG. 2. (Color) LDOS for the innermost Co layer, Co(1), for the clean Al-terminated interface. The LDOS shows typical bulklike character as expected.

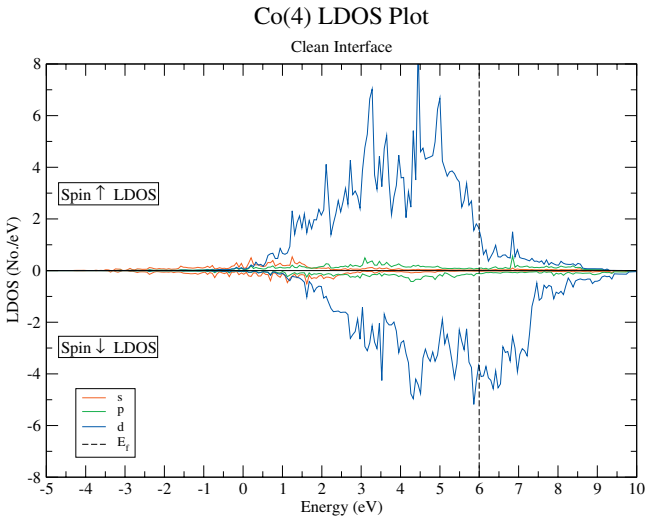

FIG. 3. (Color) LDOS for the interfacial Co layer, Co(4), for the clean Al-terminated interface.

10^{-3} eV. With this convergence criterion the residual forces were found to be less than 0.02 eV/Å for the interfacial Co or Co-Al layers. The LDOS per layer was calculated as a *spd* site-projected LDOS using the monatomic Wigner-Seitz radii and then summed over each layer, see Figs. 1 and 5 for typical layout of the layers.

III. CLEAN INTERFACE

Figure 1 shows the supercell used for calculating the properties of a clean, Al-terminated interface junction. We performed both LDA and GGA calculation but found the LDA results to be more self-consistent. For reference we also used Co in the hcp structure but could not detect any significant change from the fcc structure, which was then used throughout the rest of the work.

Figures 2–4 show the LDOS for the innermost Co layer, Co(1), the interface Co, Co(4), layer, as well as the first Al layer, Al(1). As expected, the LDOS for Co(1), which is furthest from the interface, is almost identical to that of bulk Co with an exchange splitting of ≈1.5 eV. The major peaks in the spin-up *d*-electron LDOS is below E_F, indicating that the spin-up *d* orbitals are filled as expected. Similarly, some of the spin-down *d*-electron peaks are above E_F, showing that some of the spin-down *d* orbitals are unfilled; this gives rise to the net magnetic moment. The *s* and *p* electrons also show some hybridization with the *d* electrons, as evidenced by the slight increase in the spin-up *s*- and *p*-electron density at ≈3 eV, and the spin-down *s*-electron and *p*-electron density at ≈4.3 eV.

The LDOS for Co(4), which is the layer at the interface for the clean interface, shows the effect of hybridization with the *s*-*p* electrons in the Al(1) layer next to it. The *d* electrons are more delocalized and this is reflected in that the *d*-electron peaks are not as well defined as in the Co(1) layer. The peak in the spin-up *d* band near 3 eV is reduced, and the peak near 5.6 eV has been shifted to a much smaller peak near 5 eV, and the rest of the spectral weight spectral weight has been moved to a more delocalized LDOS around 5 eV.

There is also a slight reduction in the magnetic moment in this Co(4) layer as compared to the bulklike Co(1). The spin polarization, $\delta_s = \frac{\rho_\uparrow(E_F)-\rho_\downarrow(E_F)}{\rho_\uparrow(E_F)+\rho_\downarrow(E_F)}$, for the Co(1) layer is −0.64 but −0.43 for the Co(4) layer. For this clean interface system, this is due to the hybridization between the Co *d* electrons and the Al *s*-*p* electrons at the interface. The trend of increasing positive spin polarization as the interface is approached is seen in all three systems, i.e., in both the clean interface and the two disordered interface cases which we have modeled. The detailed behavior of the spin polarization is shown in Fig. 10, and is discussed further in Sec. V.

The Al(1) layer is the start of the insulating Al_2O_3 barrier. However, due to hybridization of the Al *s*-*p* electrons with the *d* electrons in the neighboring Co(4) layer, there is a finite DOS at E_F. It is only the O(1) layer next to Al(1) that shows a gap at E_F and therefore the actual width of the

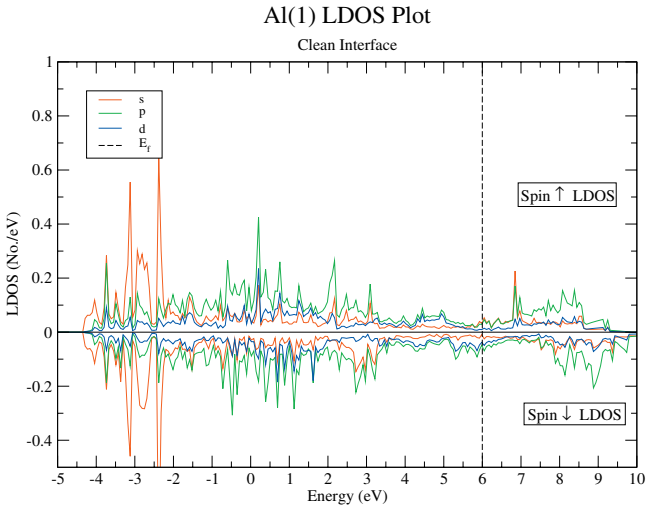

FIG. 4. (Color) LDOS for the first Al layer in the insulating barrier, Al(1), for the clean Al-terminated interface.

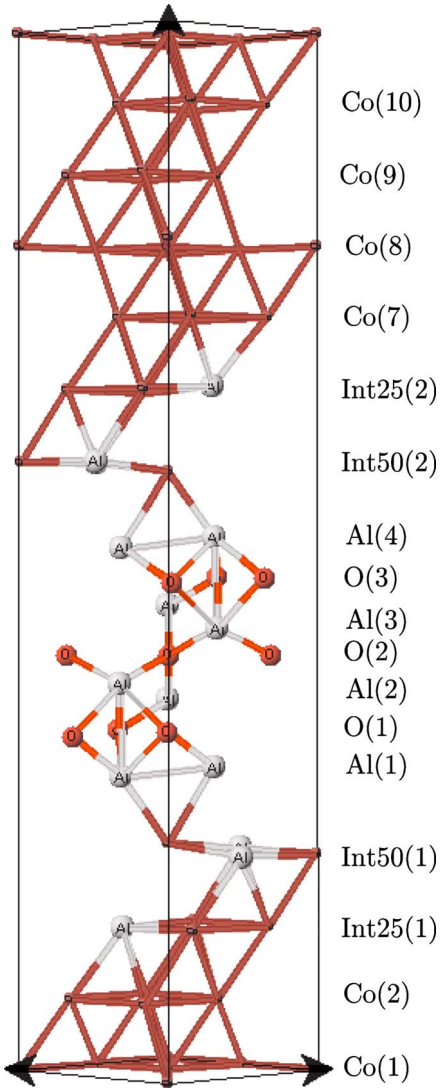

FIG. 5. (Color online) Atomic structure of a disordered Al-rich interface junction. The unit vectors for the supercell as well as the layer identification tags are shown. The Int25 layers contain a 3:1 Co to Al ratio whereas the Int50 layers have a 1:1 ratio.

insulating barrier is decreased by one to two atomic layers. Calculation of the current-voltage curves using both cases shows that a decrease by one atomic layer gives a better fit with experimental results.[16] This means that the metallization of the Al(1) and Al(4) layers in actual samples is probably only partial with a resulting decrease in tunneling width of a total of only one atomic layer.

IV. INTERFACIAL SCATTERING AND FRIEDEL SCREENING EFFECTS

From transmission electron microscopy studies of MTJ structures, it can be seen that there is atomic-level disorder at the interface.[17,18] This atomic-level disorder at the interface will necessarily result in scattering of the conduction electrons. Assuming Al termination at the interface, the Al atoms will act as positively charged impurities, because of their charge in the alumina, and this charge should get screened by the *s*-*p* and *d* electrons in the Co. From Friedel's sum rule, we know that the conduction electrons will screen the impurity charge, resulting in a change in the LDOS near the interface. Almost all of the screening will be due to the *d* electrons as the LDOS of the *d* electrons is much larger than the *s* and *p* electrons for Co at E_F. Also, since the spin-down DOS in cobalt is larger than the spin-up DOS at E_F, more spin-down electrons will be involved in the screening. This will result in a spin-dependent change in the LDOS at the interface. Similar spin-dependent charge-transfer effects have also been seen in other DFT works on clean Al-terminated interfaces, where there is a larger transfer in the spin-down band than the spin-up band.[8]

We can calculate the approximate shift in E_F and LDOS at E_F, $\delta\rho_s^o(E_F)$, for the spin-polarized *d*-electron bands, and give an estimate of the spin-dependent Friedel-screening effect.[19] We assume one Al impurity per unit cell and use the LDOS of clean Co as shown in Fig. 2. The total phase shift for both spin-up and spin-down bands must satisfy $\theta_\uparrow(E_F) + \theta_\downarrow(E_F) = \pi Z$, where Z is the charge of the impurity, so as to completely screen the impurity. The phase shift of each band, $\theta_s(\epsilon)$, is given by

$$\tan[\theta_s(\epsilon)] = \frac{\pi\rho_s^o(\epsilon)}{F_s(\epsilon) - \frac{1}{U}},$$

$$F_s(\epsilon) = P\int \frac{\rho_s^o(\epsilon')}{\epsilon - \epsilon'} d\epsilon'. \quad (2)$$

Here, U, the impurity potential, as seen by both bands is clearly the same. Since $\rho_\downarrow^o(E_F) > \rho_\uparrow^o(E_F)$, the spin-down band is expected to screen more of the impurity charge than the spin-up band. In the "rigid-band" approximation, the shift in E_F can be approximated by $\Delta_s = \frac{\theta_s}{\pi\rho_s^o(E_F)}$ and the change in the LDOS at E_F is approximated by $\delta\rho_s^o(E_F) = \Delta_s \frac{\partial\rho_s^o}{\partial\epsilon}(E_F)$. A straightforward calculation gives $\theta_\uparrow(E_F) = 0.42\pi$ and $\theta_\downarrow(E_F) = 0.58\pi$, which gives $\Delta_\uparrow = 0.30$ eV and $\Delta_\downarrow = 0.56$ eV, showing that the spin-down *d* electrons experience a Freidel screening effect that is about twice as strong. Since the tunneling current depends strongly on the DOS at E_F, this change in the LDOS will have a significant effect on the spin-polarized tunneling current.

As will be shown below, DFT results for the Al-rich interfaces clearly demonstrate the significance of hybridization and the spin-dependent Friedel screening effect. In order to obtain an accurate and reliable band structures arising from this Al-induced disorder effect, we carried out DFT calculations on interfaces with an excess amount of Al incorporated at the interface. We believe the most obvious place for these excess Al atoms are to replace Co in the Co lattice and we therefore created interfaces with Al-Co layers. As described in Sec. II we studied both junctions with one and two Co-Al interfacial layers. The case with only one interfacial layer can qualitatively be interpreted as an interpolation between the clean and the two interfacial Co-Al layer interfaces so we will for clarity and compactness only report the results on the case with two interfacial Al-Co layers. The layer spin polar-

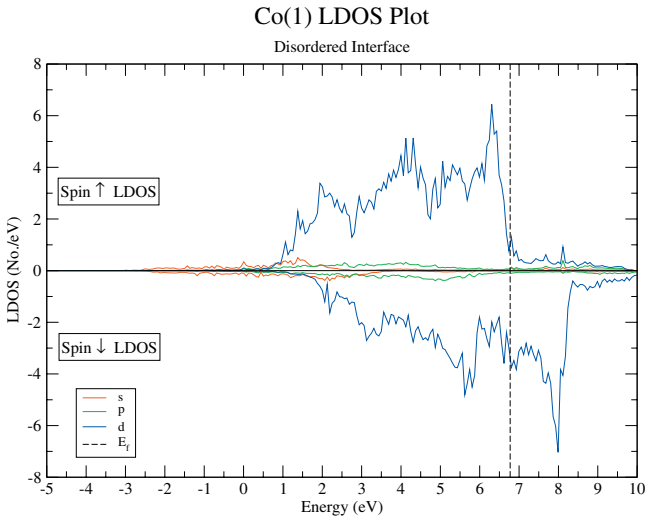

FIG. 6. (Color) Spin-dependent LDOS for Co(1) layer, for the Al-rich disordered interface.

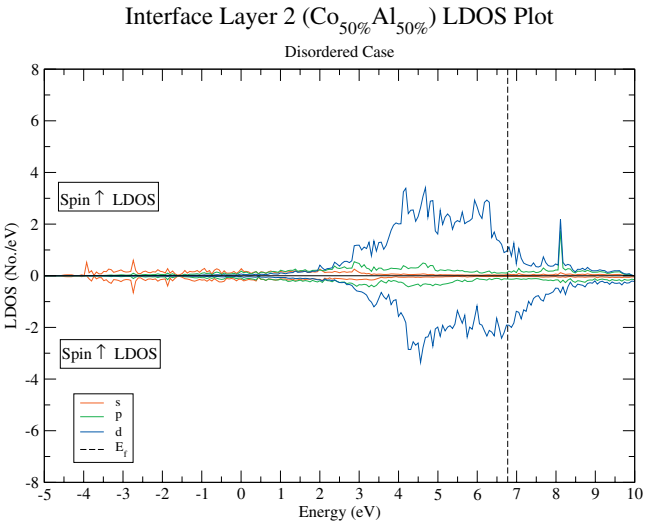

FIG. 8. (Color) Spin-dependent LDOS for second interface layer, Int50(1), with the ratio Co:Al=1:1.

ization in Fig. 10, which includes the results for all three structures, clearly shows the intermediate features for the one interfacial layer structure.

V. Al-RICH DISORDERED INTERFACE

The self-consistent atomic structure of the supercell for modeling the Al-rich disordered interface, with interface layers Int25 and Int50, is shown in Fig. 5. The first interface layer Int25(1), i.e., the layer closest to the Co substrate, has a 3:1 ratio of Co to Al, and the second mixed layer Int50(1), which is next to the Al(1) layer, has a 1:1 ratio of Co to Al. In Figs. 6–9 we plot the spin-dependent LDOS for the first Co layer, Co(1), the first interface layer, Int25(1), the second interface layer, Int(50), and the first Al layer, Al(1), respectively, to show the change in spin-dependent LDOS as we approach and cross the interface. Comparing these results with those from Sec. III, we are able to see the effects of Friedel screening of Al atoms at the disordered interface.

As expected, the LDOS for Co(1) is almost the same as bulk Co and the Co(1) layer of the clean interface case, giving an exchange splitting of ≈ 1.5 eV. The LDOS of Co(1) shows a large spin-down polarization at E_F, with $\rho_\uparrow(E_F) \approx 1$ eV^{-1} and $\rho_\downarrow(E_F) \approx 4$ eV^{-1}, similar to that of the clean interface case. This means the screening length for the interfacial disorder effects is very short, of about one atomic layer, as expected for a metal.

The mixing of Al and Co in the disordered layers near the interface results in spin-dependent Friedel screening, which changes the LDOS. Since $\rho_\downarrow(E_F) > \rho_\uparrow(E_F)$ for bulk Co and also in the Co(1) layer, screening of the Al atoms in the Int25 and Int50 layers would be mostly from the spin-down d electrons. Therefore $\rho_\downarrow(E_F)$ should change proportionally more than $\rho_\uparrow(E_F)$, as shown in the calculation for the Friedel screening.

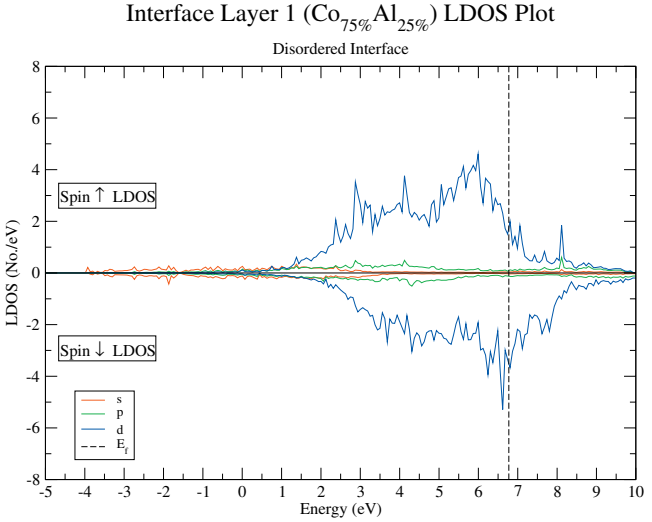

FIG. 7. (Color) Spin-dependent LDOS for first interface layer, Int25(1), with the ratio Co:Al=3:1.

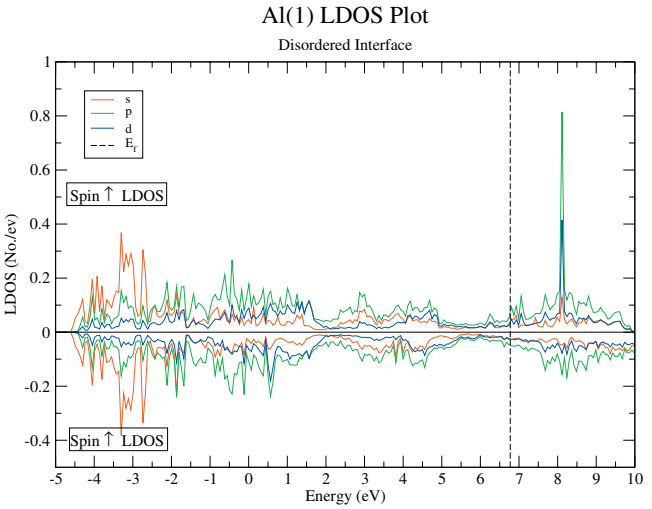

FIG. 9. (Color) Spin-dependent LDOS for first Al layer, Al(1), for the Al-rich disordered interface.

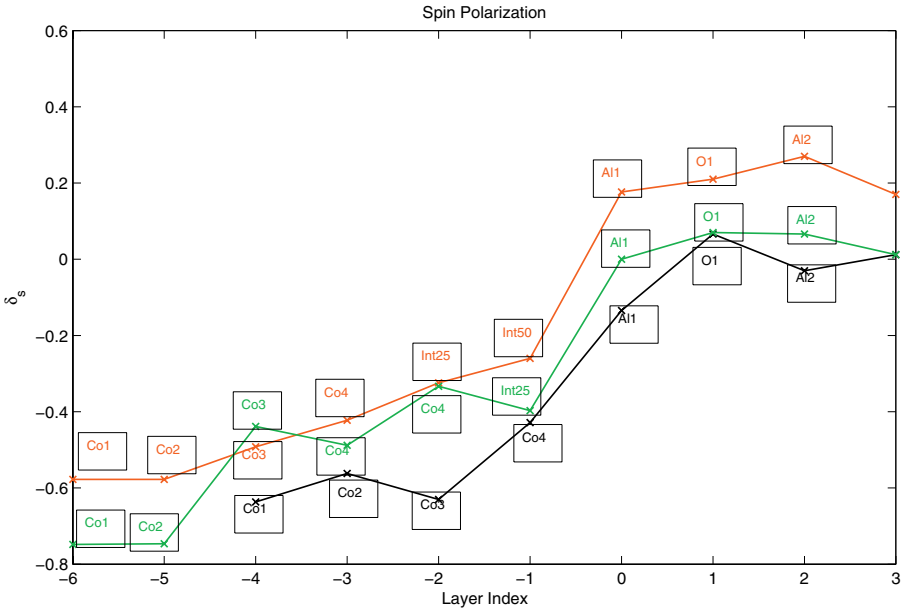

FIG. 10. (Color) Spin polarization at E_F, $\delta_s(E_F)$, of the three different MTJ structures investigated assigning the Al(1) layer to be layer 0. Clean interface (black), one Co/Al interfacial layer (green), and two Co/Al interfacial layers (red).

The effects of the spin-dependent screening are seen in both the LDOS near E_F and the total number of d electrons per layer. There is a large change in the LDOS at E_F for the Int50 layer compared to the Co(1) layer, which has significant importance for tunneling transport. For the Int50 layer, $\rho_{d\uparrow}=1.0$ eV^{-1} and $\rho_{d\downarrow}=1.9$ eV^{-1}. Comparing this to the bulklike layer of Co(1) where $\rho_{d\uparrow}=1.0$ eV^{-1} and $\rho_{d\downarrow}=3.4$ eV^{-1}, we see that there is clearly a much larger change in the spin-down LDOS. The spin-up LDOS is unchanged while the spin-down LDOS is almost reduced by half. Similarly, there is a much larger change for the total spin-down d electrons in the Int50 layer. The total d electron charge in the Int50 layer is 8.4 eV^{-1}/layer and 7.2 eV^{-1}/layer for spin up and spin down, respectively. In comparison, the average of the Al(1) and Co(1) layers is 9.0 eV^{-1}/layer and 6.0 eV^{-1}/layer, respectively, for spin up and spin down. This shows the spin-dependent change in the LDOS of the interfacial layers is due to screening effects, whereas hybridization should lead to a similar change in the LDOS for both spins.

In addition, we have calculated the average of the LDOS of the Co(1) and Al(1) layers in the clean case to obtain an estimate for the effects of hybridization, and compared that to the Int50 LDOS for a clearer picture of the effects of the spin-dependent screening. The LDOS near E_F for the two are very similar for spin up, whereas spin down shows a large shift of spectral weight from around E_F to the peak seen in Int50 at about 4.6 eV. This leads to the change in the spin polarization at E_F and also affects the spin-polarized tunneling current, both of which are discussed further in the following sections.

The sharp peaks in the d-electron LDOS that were seen in the Co(1) layer are also significantly reduced in the Int25 and Int50 layers, indicating that the d-electron orbitals are more delocalized. This is due to hybridization with the Al s-p bands from the neighboring Al(1) layer, and with the Al s-p electrons in the layers itself.

We notice that the first Al layer, Al(1), has a small but finite LDOS at E_F, since it has become metallized by proximity to the Co layers, an effect also seen for the clean interface. The effective insulating width of the Al_2O_3 layer is therefore again reduced by approximately one atomic layer.

We plot in Fig. 10 the spin polarization, δ_s, of the three different Al-terminated MTJ structure studied, starting in the bulk and moving across the interface into the Al_2O_3 insulating barrier. Due to the periodicity of the supercell in the DFT simulation, the Co(1) and Co(2) layers, and the Co(9) and Co(10) layers that are not shown, are the bulklike layers for the two systems with a disordered interface. As we approach the interface we can see an increase in δ_s of each layer. The bulk Co layers have a $\delta_s \approx -(0.6-0.8)$ in all structures. For

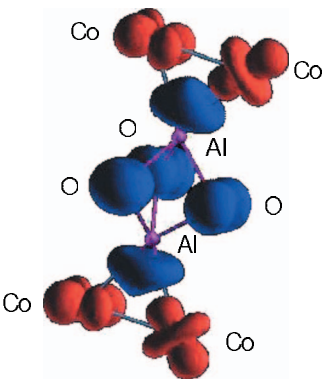

FIG. 11. (Color) Atomic structure of model system of nine atoms representing the Al-terminated Co/Al_2O_3/Co MTJ structure. The figure shows the total spin polarization and the color indicates the spin polarization for each atom. The Al atom is positively spin polarized and the Co atom is negatively spin polarized. This result is due to a kinetic exchange process. Matching so closely the larger calculation, it is suggestive that a kinetic exchange process is also responsible for the positive spin polarization in the larger structure.

TABLE I. Effective-mass values (m/m_0) for the different electron bands in the cobalt layer, the interface layer, and the insulating Al_2O_3 layer. Notice the large change in the effective mass for the spin-down d2 bands between the Co(1) and the Int25/Int50 layers.

	Co(1) layer				Int25/Int50 layer			Al_2O_3 layer
Bands	*s-p*	d1	d2	d3	*s-p*	d1	d2	*s-p*
Spin ↑	0.45	0.81	2.05	6.19	0.51	0.81	1.70	1.0
Spin ↓	0.37	1.02	4.99	7.89	0.51	0.58	1.70	1.0

both the clean and disordered system, δ_s increases as we approach the interface. For the clean Al-terminated interface the spin polarization remains slightly negative at the interfacial Al(1) layer and becomes slightly positive in the O(1) layer. For the two interfacial layer structures (Fig. 5) the spin polarization similarly increases toward the interface, $\delta_s = -0.32$ in the Int25 layer, and $\delta_s = -0.27$ in the Int50 layer. Furthermore, the spin polarization becomes positive, $\delta_s = 0.2$, at the metallized interfacial Al(1) layer.

Looking at the change in spin polarization from the bulk-like Co(1) layer to the layer at the interface, the increase in δ_s from the Co(1) to Co(4) layer for the clean interface system can be attributed solely to hybridization with the Al *s-p* electron in the Al(1) layer. For this system, the spin polarization changes from -0.64 to -0.43, which is a change of 33%. On the other hand, for the disordered system with two mixed layers, δ_s increases from -0.58 to -0.26 between the Co(1) and the Int50 layer, which is a change of 55%. This clearly shows the additional effects of the spin-dependent Friedel screening and interfacial disorder on the spin polarization.

We have also calculated the magnetic moment for each layer, for both the clean and disordered interface systems. The magnetic moment decreases monotonically, and is reduced by 15% from the bulk value at the Co(1) layer to the Co(4) layer at the clean interface, with most of the reduction occurring in the two layers nearest to the interface. Similar results are obtained from the disordered interface system.

To study the source of the positive spin polarization in the interface region shown in Fig. 10, we have performed a calculation on a model system, an "essential unit cell" of the interface region, shown in Fig. 11. This is composed of an Al atom bonded to two Co atoms in one direction and to three oxygen in the other. These oxygen are bonded to a second Al and the structure simplified by termination at this point with two final Co. The bond lengths and angles were chosen to match those of the clean structure, Fig. 1. For reasons shown in the following discussion, we believe the model structure may capture much of the essence of the spin interactions and hybridization at the interface.

Density-functional calculations were performed on this system in a comparable manner to those in the rest of this paper, including full relaxation of the structure. The program QUANTUM ESPRESSO (Ref. 20) was used with convergence and other properties similar to those described in Sec. II. Relaxation of the structure did not change the bond lengths or angles from those of the full calculation of Fig. 1.

Figure 11 shows the spatial distribution of the spin polarization with contrasting color indicating opposite direction of spins. We note first of all the marked similarities between these results and those of Fig. 10. The total spin polarization on both the Al and O layers is positive, opposite to the negative spin polarization of the Co. In addition, the spin polarization of the Al is not centered on the Al itself, but rather is midway to the Co, indicating the extent of the hybridization. Both the Al and Co polarizations have a marked anisotropy, indicating the preferential involvement of certain orbitals in the development of the spin polarization.

Al draws electrons from the Co, a process akin to Friedel screening in a larger system. The electrons are then spin polarized in the opposite direction to Co due a kinetic exchange process. The system lowers its kinetic energy via kinetic exchange; i.e., hopping of the spin-down electron from the Co atom onto a virtually excited state of the spin-up polarized Al atom, and back onto the Co atom. There is also a superexchange interaction occurring in this small system between the two Co atoms via the Al.[21] Similarly we find in the full MTJ structure, shown in Fig. 1, that the Al has a total spin polarization opposite to the Co atom. We suggest this is due to similar Pauli exclusion effects in the screening process. If the MTJ structure is O terminated instead, the interfacial O atoms would behave similarly to the interfacial Al atoms that we have described above; i.e., the O atom would be screened by the Co electrons and would have a net positive total spin polarization.

The spin-polarization results for the three different Al-terminated systems shown in Fig. 10 shows explicitly that not only a O-rich but also a Al-rich disordered interface can give rise to a positive spin polarization in the insulating alumina layer. Moreover, this positive spin polarization can be reached in a region with a finite LDOS at the Fermi level for an Al-rich interface, namely, the Al(1) layer, which is of crucial importance when studying tunneling processes. The effects of the change in spin polarization on the tunneling current is modeled using spin-dependent effective masses for the different bands in each layer as discussed the section below. This is shown in Table I, especially for the d2 bands, which contribute the most to the LDOS at E_F. The details of the effective-mass derivations and effects on the tunneling current are discussed in Sec. VI.

VI. SPIN-POLARIZED TUNNELING CURRENT

In this section, we show how the net positive spin polarization at the interface leads to a positively spin-polarized tunneling current. Using a straightforward tunneling Hamiltonian that models the finite gap in the band structure of the Al_2O_3 layers, and effective-mass values directly extracted from the DFT calculations, we calculate that the tunneling

current is positively spin polarized. This is due to the large change in spin-down LDOS between the bulklike and interface layers, resulting in a greater mismatch in effective-mass values; hence the spin-down electrons have a smaller transmission coefficient. Our fundamental model thus enables physical insight into the relation between the spin polarization of the LDOS and the tunneling current. Furthermore, we are able to obtain reasonable agreement in the polarization values with experiments, i.e., calculated value of 53% compared to an experimental value of 42%.

The position-dependent effective-mass model is solved numerically to obtain the tunneling current. The tunneling layer is modeled in the standard manner as a potential barrier, V_o, with thickness a, and applied voltage V_1. The Hamiltonian for the system is written simply as an effective kinetic mass term and a potential barrier,

$$H = \frac{p^2}{2m(x)} + \theta(x)\,\theta(a-x)\left(V_0 - \frac{V_1}{a}x\right). \tag{3}$$

The effective mass, $m(x)$, changes discontinuously from layer to layer, and the values for the different *s-p* and *d* bands are obtained from the DFT calculations as described below. The Fermi energy is 6.78 eV, as determined from the LDA results, the effective barrier height, V_0=9.4 eV, is obtained from electron spectroscopy of thin-film Al_2O_3 layers.[22] The effective width of the Al_2O_3 layer, a, is taken to be one atomic layer thinner than the actual thickness shown in Fig. 5, due to the partial metallization of the Al layers at the interface. The appropriate boundary conditions to be imposed between every layer is

$$\psi(0-) = \psi(0+),$$

$$\frac{1}{m_1}\frac{d\psi}{dx}(0-) = \frac{1}{m_2}\frac{d\psi}{dx}(0+), \tag{4}$$

where m_1 is the effective mass for the layer on the left, $x<0$, and m_2 is the effective mass for the layer on the right, $x>0$, where $x=0$ is where the layers meet.

We extract effective masses for our model from the DFT results as follows. The DFT LDOS data is decomposed into *s-p* and *d* bands for each of the layers, which we model separately with different effective-mass values. The *d*-electron band is modeled using three bands, d1, d2, and d3, so as to more realistically capture the LDOS near E_F. First, we project the DFT LDOS data into *s-p* and *d* bands for each of the layers and, in particular, look at the data near E_F. Next, we model the *d*-electron band as three separate bands in order to more accurately capture the LDOS near E_F. The large peak near E_F is modeled using one band, labeled as d3, the overall large-effective-mass *d* band is modeled using another band, labeled as d2, and a more flat *sp*-like band is labeled as d1. We model the *s-p*, d1, d2, and d3 bands with a free-electron density-of-states expression, with effective mass, m^*, and the band edge as fitting parameters.

To check our results, we also use the full LDA band structure to extract the Fermi velocity, v_F, for each band and then use $v_F=\frac{k_F}{m^*}$ to extract an effective mass, m^* for each of the bands. We find that the effective masses, m, extracted from the free-electron picture above are in good agreement with the band-structure masses, m^*, and thus we have a high confidence in our approach. The effective masses, with respect to the bare electron mass m_0, are shown in Table I. Here the two disordered layers at the interface, Int25 and Int50, are treated as one single layer for ease of calculation. The LDOS of the two layers are similar and the effective-mass value used is the average of the effective masses obtained from the two layers. The d3 bands in the interface layers do not cross E_F and are therefore assumed to be irrelevant for the transport calculations.

The increase in the spin polarization due to the Al-rich interface is reflected in the spin-dependent effective masses of the *d*-electron bands, especially in the d2 bands which has the largest LDOS at E_F. It is shown in Table I that the d2 bands in the Co(1) layer have effective masses $2.05m_0$ and $4.99m_0$ for spin up and spin down, respectively, which both reduce to $1.70m_0$ in the interface layer. Clearly the larger decrease in spin-down LDOS near E_F, due to the Friedel screening effect and LDA results shown in Secs. IV and V, leads to a corresponding increase in spin polarization $\delta_s(E_F)$. This decrease in LDOS is modeled by the change in the effective-mass values from the Co(1) layer to the interface layers. A smaller tunneling probability for the spin-down *d* bands hence results, due to the larger spin-down effective masses, and the greater mismatch in effective masses between the Co(1) and the Int25/Int50 layer. This is clearly seen for all three d1, d2, and d3 bands, and hence there is a smaller spin-down polarized tunneling current.

The exact wave functions for the Hamiltonian, Eq. (3), are described by Airy functions whose coefficients are determined numerically using the boundary conditions, Eq. (4), and a normalization condition for the wave function. The numerically determined wave function is then used to calculate the tunneling probabilities and tunneling current which is given by the standard current expression,

$$j = i\hbar\left[\frac{\partial\psi(x)}{\partial x}\psi^*(x) - \frac{\partial\psi^*(x)}{\partial x}\psi(x)\right]. \tag{5}$$

Figure 12 shows the tunneling current for the parallel configuration, where the magnetization of the two cobalt layers are parallel. Therefore, the spin-up electrons tunnel to the spin-up bands, and similarly for the spin-down electrons. The *s-p* band electrons naturally tunnel to the *s-p* band by symmetry, and since the d1, d2, and d3 band electrons were originally modeled from the same *d*-electron band, they tunnel into the other bands as well; i.e., the d1 band electrons tunnel into the d2 and d3 bands as well as the d1 band.

The spin-polarized tunneling for both the *s-p* electrons and the *d* electrons are positive, up to $\approx$0.9 eV. The positive spin-polarization tunneling current arises from a greater mismatch in the effective masses of the spin-down bands between the bulk cobalt layer, Co(1), and the interface layers as compared to a smaller mismatch in the spin-up bands. This is also seen in the *s-p* bands, where there is a slightly better match between the spin-up effective masses. This results in a slightly larger spin-up tunneling current for the spin-up *s-p* band, as shown in Fig. 12. There is also a large peak, modeled as the d3 band, in the LDOS of spin-up *d* electrons,

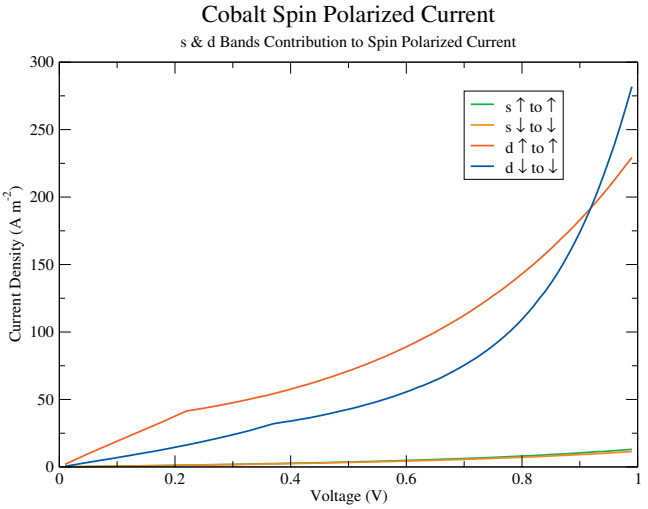

FIG. 12. (Color) Spin-polarized tunneling current of MTJ structure. The lower transmission coefficient for the spin-down bands, due to a greater mismatch in effective masses, result in a lower tunneling current compared to the spin-up bands.

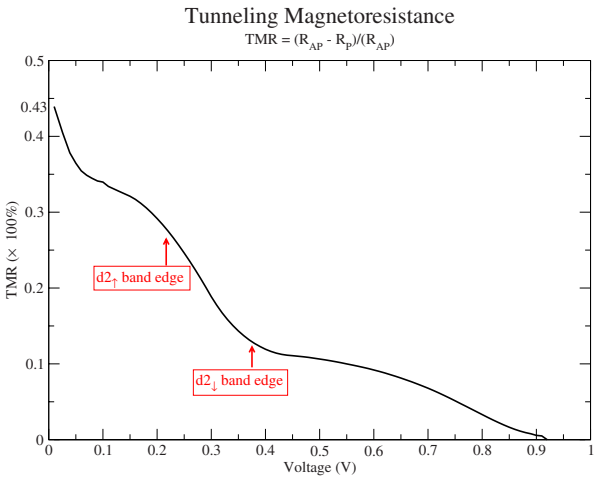

FIG. 13. (Color online) Tunneling magnetoresistance of MTJ structure calculated from Julliere's formula with spin polarization obtained from spin-polarized tunneling current shown in Fig. 12.

approximately 100 meV below E_F, that affects the spin-polarized tunneling; whereas a similar peak for the spin-down d electrons is 1.26 eV above E_F due to the exchange splitting. This is seen clearly in Fig. 6. Therefore, for an applied voltage larger than 100 meV, this large spin-up d3 band will contribute, and results in a larger spin-up polarized tunneling current. This continues until 0.91 eV, when the bottom of the spin-down d3 band crosses the quasi-Fermi level and starts to contribute to tunneling. The positive spin-polarized tunneling current reflects the positive spin polarization shown in Fig. 10 as we cross from the cobalt layers into the Al_2O_3 layer and explains the positive spin polarization found experimentally.

Finally, we can numerically calculate the tunneling spin polarization, $P=\frac{I_\uparrow - I_\downarrow}{I_\uparrow + I_\downarrow}$, where $I_{\uparrow,\downarrow}$ is the spin-polarized tunneling current given in Fig. 12. Using Julliere's formula, Eq. (1), we then calculated the TMR from the numerically derived tunneling spin polarization P, and the results are shown in Fig. 13.

The calculated spin polarization is $P=53\%$, which compares very well with the experimental values of 42% for Co and 55% for $Co_{50}Fe_{50}$.[5,23] The calculated TMR is 43% at zero applied voltage, which compares favorably with the experimental value of 30%. Next, we see that the TMR decreases monotonically with applied voltage and reaches zero at 0.91 V. The spin polarization and TMR both decrease to zero at this voltage, which is the spin-down d3 band edge and is on the order of the exchange splitting. Finally, we also see two well-defined "roll-overs" in the TMR curve labeled "$d2_\uparrow$ band edge" and "$d2_\downarrow$ band edge." This is due to band-structure effects; the first "roll-over" at 0.23 V is due to the spin-up d2 band edge and the second "roll-over" at 0.375 V is due to the spin-down d2 band edge, where the two bands stop contributing to the tunneling transport. The monotonic decrease in TMR with increase in voltage and the roll-overs have been seen experimentally, see, e.g., Refs. 2, 24, and 25. These two roll-overs are much more prominent in the numerical results because the band edges for the $d2_\uparrow$ and $d2_\downarrow$ bands in the effective-mass model are modeled using step functions, which is more abrupt than the real band structure.

VII. CONCLUSIONS

In this paper, we have studied the effect of interface mixing and atomic-level disorder on the spin-polarized tunneling current in Co/Al_2O_3 MTJs. The spin polarization of tunneling currents in MTJs have clearly been seen in experiments to be positive at odds with simplistic tunneling models which depends on the spin polarization of the DOS at the Fermi energy of the leads. There is now a growing body of evidence that interface effects at the boundary between the Co layers and the aluminum oxide insulating layer play an important role in determining the spin-polarized transport in these systems. A large number of studies have assumed an O-rich interface and found positive spin polarization for such systems. However, we believe that an Al-rich/terminated interface is more relevant experimentally when the junction is not heavily oxidized.

The MTJ was modeled realistically using DFT in both the LDA and GGA approximations, of which the LDA scheme was found to be more consistently reliable. While a nonamorphous structure of the alumina is necessary in any supercell approach we do not expect this approximation to significantly change our conclusions. We have studied both clean Al-terminated and Al-rich disordered interface systems, and found a consistent trend of increasing positive spin polarization with Al content of the interface. The main effects of the Al-rich disordered interface are spin-dependent Freidel screening of the Al impurities in the interface lead layers, and hybridization with the s-p electrons of the Al impurities and the neighboring first Al layer of the insulating barrier. This causes a much larger change in the spin-down d-electron LDOS near E_F of the interface layers, leading to an increase in the spin polarization near E_F. Another important result of our LDA calculations is that the proximity effect leads to metallization of the first Al layer by the neigh-

boring Co layer. This reduces the effective width of the insulating layer and can be seen in the slope of the *I-V* curve.

Studying the interface with a model system which focuses on the Co-Al-O interactions, we find good agreement with the larger calculation on the incidence and sign of spin polarization in the interface layers. This model calculation suggests that the source of the opposite polarization of the Al and O is an exchange mechanism similar to that seen with magnetic atoms on an insulating surface.[26] Just as the Ruderman-Kittel-Kasuya-Yoshida (RKKY) interaction was originally studied with isolated magnetic impurities in bulk metals, and then widely seen in metallic magnetic multilayers, we postulate that the exchange interactions, both kinetic and superexchange, previously seen for isolated magnetic atoms separated by a nonmagnetic insulating "island" are also applicable to many magnetic tunnel junctions.

The effects of increasing spin polarization in the LDOS near E_F is captured using a layer- and spin-dependent effective-mass model, which is used to calculate the tunneling current. The greater mismatch of the effective masses leads to a smaller transmission coefficient for the spin-down *d* bands and the tunneling current clearly shows a positive spin polarization that is in agreement with experimental results. This defines an effective tunneling spin polarization, which allowed us to calculate the TMR using the Julliere model, giving results that are also in good agreement with experiments.

In summary, using DFT calculations, we have found that Al-terminated interfaces in MTJs show positive spin polarization of the LDOS at E_F, showing that positive spin polarization is possible not only in O-terminated MTJ systems. Furthermore, we formulated a spin-dependent effective-mass model, using values extracted from the DFT results, that was used to calculate the tunneling current and the TMR. The results clearly show a positive spin polarization and TMR values that are in agreement with experiments. Thus, our model demonstrates how positive spin polarization and realistic TMR values can be obtained in an Al-terminated MTJ. Future work could include a time-dependent DFT study or evanescent decay rate model,[27] which would be able to study the transport properties in more detail.

ACKNOWLEDGMENTS

We thank Shu Peng and Kyeongjae Cho for invaluable help in the beginning of this work. We would also like to thank Stuart Parkin and his group members for very helpful discussions and unpublished data. T. Tzen Ong was partly funded by IBM and partly by the CPN Stanford. W. Shen was funded by NSF under Grant No. DMR-0705266.

*Present address: Nordita, Roslagstullsbacken 23, SE-106 91 Stockholm, Sweden.

[1] J. S. Moodera, L. R. Kinder, T. M. Wong, and R. Meservey, Phys. Rev. Lett. **74**, 3273 (1995).
[2] J. S. Moodera, J. Nassar, and G. Mathon, Annu. Rev. Mater. Sci. **29**, 381 (1999).
[3] E. Y. Tsymbal, O. N. Mryasov, and P. R. LeClair, J. Phys.: Condens. Matter **15**, R109 (2003).
[4] M. Julliere, Phys. Lett. A **54**, 225 (1975).
[5] R. Meservey and P. M. Tedrow, Phys. Rep. **238**, 173 (1994).
[6] P. LeClair, J. T. Kohlhepp, H. J. M. Swagten, and W. J. M. de Jonge, Phys. Rev. Lett. **86**, 1066 (2001).
[7] P. LeClair, J. T. Kohlhepp, C. H. van de Vin, H. Wieldraaijer, H. J. M. Swagten, W. J. M. de Jonge, A. H. Davis, J. M. MacLaren, J. S. Moodera, and R. Jansen, Phys. Rev. Lett. **88**, 107201 (2002).
[8] I. I. Oleinik, E. Y. Tsymbal, and D. G. Pettifor, Phys. Rev. B **62**, 3952 (2000).
[9] I. I. Oleynik and E. Y. Tsymbal, J. Appl. Phys. **93**, 6429 (2003).
[10] K. D. Belashchenko, E. Y. Tsymbal, I. I. Oleynik, and M. van Schilfgaarde, Phys. Rev. B **71**, 224422 (2005).
[11] N. D. Telling, G. van der Laan, S. Ladak, R. J. Hicken, and E. Arenholz, J. Appl. Phys. **99**, 08E505 (2006).
[12] M. Bowen, V. Cros, H. Jaffrès, P. Bencok, F. Petroff, and N. B. Brookes, Phys. Rev. B **73**, 012405 (2006).
[13] M. J. Plisch, J. L. Chang, J. Silcox, and R. A. Buhrman, Appl. Phys. Lett. **79**, 391 (2001).
[14] I. I. Mazin, Phys. Rev. Lett. **83**, 1427 (1999).
[15] G. Kresse and J. Furthmüller, Comput. Mater. Sci. **6**, 15 (1996).
[16] A. Panchula and S. S. P. Parkin (private communication).
[17] J. S. Bae, K. H. Shin, T. D. Lee, and H. M. Lee, Appl. Phys. Lett. **80**, 1168 (2002).
[18] X. Portier, A. K. Petford-Long, J. H. Nickel, and J. A. Brug, Appl. Phys. Lett. **79**, 57 (2001).
[19] S. Doniach and E. H. Sondheimer, *Green's Functions for Solid State Physicists* (Imperial College Press, London, UK, 1999), see Chap. 4 for a discussion of the Friedel sum rule.
[20] S. Baroni, A. D. Corso, S. de Gironcoli, and P. Giannozzi (unpublished). Please see http://www.QuantumEspresso.org
[21] A. Bencini and D. Gatteschi, *EPR Exchange Coupled Systems* (Springer-Verlag, New York, NY, 1990).
[22] I. Costina and R. Franchy, Appl. Phys. Lett. **78**, 4139 (2001).
[23] R. J. M. van de Veerdonk, J. S. Moodera, and W. J. M. de Jonge, in Conference Digest of the 15th International Colloquium on Magnetic Films and Surfaces, Queensland, 1997 (unpublished).
[24] J. S. Moodera, J. Nowak, and R. J. M. van de Veerdonk, Phys. Rev. Lett. **80**, 2941 (1998).
[25] E. Nakashio, J. Sugawara, S. Onoe, and S. Kumagai, IEEE Trans. Magn. **36**, 2812 (2000).
[26] C. F. Hirjibehedin, C. P. Lutz, and A. J. Heinrich, Science **312**, 1021 (2006).
[27] U. Lüders *et al.*, Phys. Rev. B **76**, 134412 (2007).